Meshless solution of 2D and 3D Stokes flow using the radial basis integral equation method

E. H. Ooi & V. Popov
Environmental and Fluid Mechanics, Wessex Institute of Technology, UK

Abstract

The calculation of boundary vorticity, which requires the evaluation of the spatial derivatives of the velocity vector, remains a critical step when solving the fluid flow problems in the velocity-vorticity formulation. An accurate estimation of these quantities is required in order to obtain accurate numerical solution and convergence of the numerical scheme. The radial basis integral equation (RBIE) method is a meshless method that solves for each node the unknown potential and its spatial gradients. This unique feature of the RBIE makes it an efficient numerical tool for solving the fluid flow problems in the velocity-vorticity formulation, since the velocity derivatives are directly obtained from the system of equations. In this study, the efficiency of the RBIE for solving the Stokes flow problems in 2D and 3D is investigated. The accuracy of the numerical results was assessed by comparing it with the solutions obtained using the finite element method. Numerical results showed that the RBIE can be used to efficiently and accurately solve Stokes flow problems.
Keywords: meshless methods, viscous flow, velocity-vorticity formulation, RBIE, dual reciprocity method.

1 Introduction

One of the most important steps when solving Stokes flow problems in the velocity-vorticity formulation is the calculation of the boundary vorticity to be used as boundary conditions in the vorticity transport equation. An accurate estimation of the boundary vorticity not only yields an accurate numerical solution but guarantees convergence in the numerical scheme. The vorticity of a given velocity field is defined by the curl of the velocity vector. Consequently,

calculation of the boundary vorticity would require the evaluation of the spatial derivatives of the velocity vector.

The radial basis integration equation (RBIE) method is a meshless technique introduced recently by Popov and Bui [1]. The RBIE involves the distribution of nodes over the boundary and interior of the solution domain. A circular (spherical in 3D) subdomain centred on each node is then generated. One of the unique features of the RBIE is that it solves at each node for the potential and its spatial derivatives by using three (four in 3D) equations at each collocation node. In problems where the knowledge of the spatial gradients is of primary importance, such as in the calculation of the boundary vorticity, the RBIE provides a simple and straightforward numerical tool since the values of the spatial gradients at each node are obtained directly from the solution of the system of equations. This is the main focus of investigation in the present study, where the RBIE is used to solve 2D and 3D Stokes flow expressed in the velocity-vorticity formulation. The accuracy of the numerical solution is assessed by comparing the solutions with those obtained using the finite element method (FEM). In the next section, the derivation of the RBIE to solve the Stokes flow problem is presented briefly. The implementation of the numerical scheme is outlined in Section 3. This is followed by the results in Section 4 and conclusions in Section 5.

2 Mathematical formulations

2.1 Stokes flow

The governing equation for the steady-state Stokes flow expressed in the velocity-vorticity formulation in the domain Ω bounded by the close boundary Γ is given by

$$\nabla^2 \omega_i(r) = 0, \quad \text{for } r \in \Omega \cup \Gamma,$$
$$\nabla^2 u_i(r) = -\nabla \times \omega_i, \quad \text{for } r \in \Omega \cup \Gamma, \tag{1}$$

where $r = x_i$ (for $i = 1$ and 2 in 2D; for $i = 1, 2$ and 3 in 3D) are the field points in the Cartesian coordinate system, u_i is the velocity vector and ω_i is the vorticity vector. In 2D, only the ω_3 component of the vorticity exists. The first line in (1) is the vorticity transport equation, which represents the kinetic part of the flow while the second line is the velocity Poisson equation, which represents the kinematics part of the flow.

To complete the problem definition, the following boundary conditions are applied:

$$u_i(r) = U_o, \quad \text{for } r \in \Gamma, \tag{2a}$$

$$\omega_i(r) = \nabla \times u_i, \quad \text{for } r \in \Gamma, \tag{2b}$$

where U_o is a suitably prescribed function. Equation (2b), which is the mathematical definition of the vorticity vector, is calculated from the spatial derivatives of u_i obtained from solving the velocity Poisson equations.

2.2 The radial basis integral equation method

To carry out the RBIE, N_t collocation nodes are distributed over the boundary and the interior of the solution domain. A circular (spherical in 3D) subdomain Ω_s with local boundary Γ_s centred on each node is generated, see Figure 1a.
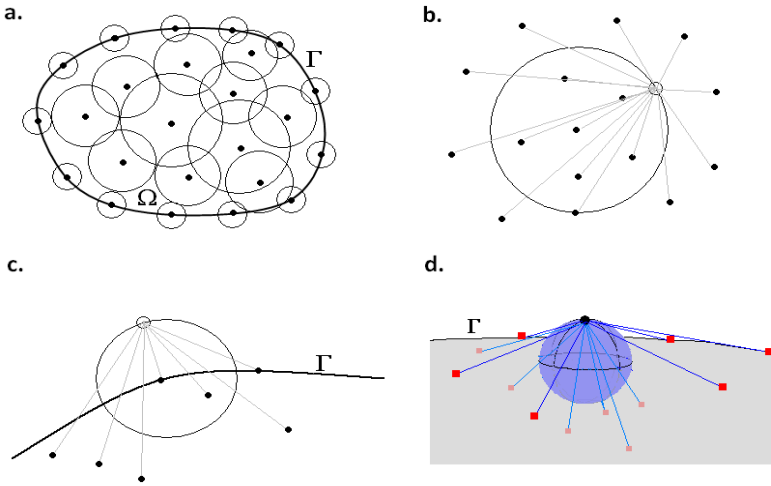

Figure 1:   (a) Collocation of nodes and selection of subdomains; (b) interpolation of unknown field variables; and extrapolation of unknown field variables exterior to the solution domain in (c) 2D and (d) 3D.

In each subdomain, the following integral equation applies:

$$\theta(r)\big|_{r=\xi} = \int_{\Gamma_s}\left(\theta(r)\frac{\partial\Phi(r;\xi)}{\partial n} - \Phi(r;\xi)\cdot n_i(r)\cdot\frac{\partial\theta}{\partial x_i}\right)d\Gamma + \int_{\Omega_s} b\cdot\Phi(r;\xi)d\Omega, \tag{3}$$

where ξ is the coordinate of the source point, θ represents each component of the vorticity and the velocity in the vorticity transport equation and the velocity Poisson equations, respectively, b is the source term, such that $b = 0$ for the vorticity transport equation and $b = -\nabla \times \omega_i$ for the velocity Poisson equations and $\Phi(r;\xi)$ is the fundamental solution of the Laplace equation.

The additional equations used for solving the spatial derivatives of the field variables are obtained by differentiating (3) yielding [1]

$$\frac{\partial\theta(r)}{\partial x_i}\bigg|_{r=\xi} = \int_{\Gamma_s}\theta(r)\frac{\partial^2\Phi(r;\xi)}{\partial x_i\partial n} - \frac{\partial^2\Phi(r;\xi)}{\partial x_i}\cdot n_i(r)\cdot\frac{\partial\theta}{\partial x_i}d\Gamma$$
$$+ \frac{\partial}{\partial x_i}\int_{\Omega_s} b\cdot\Phi(r;\xi)d\Omega, \tag{4}$$

where the partial derivatives $\partial/\partial x_i$ are calculated with respect to the source point ξ. In writing (3) and (4), the following relationship has been utilized:

$$\frac{\partial \theta}{\partial n} = n_i \cdot \frac{\partial \theta}{\partial x_i}.$$ (5)

By carrying out the radial basis function (RBF) approximations on the variables $\theta(r)$ and $\partial\theta(r)/\partial x_i$, i.e.

$$\theta(r) = \sum_{n=1}^{N_a} f(r;r^{(n)})\alpha^{(n)}; \quad \frac{\partial \theta(r)}{\partial x_i} = \sum_{n=1}^{N_a} f(r;r^{(n)})\beta^{(n)},$$ (6)

where $f(r;r^{(k)})$ is the RBF and α and β are unknown coefficients to be determined; and applying the dual reciprocity method (DRM) [2] onto the domain integrals, (3) and (4) may be expressed as

$$\theta(r)\big|_{r=\xi} = \sum_{n=1}^{N_a} \theta^{(n)} \sum_{k=1}^{N_a} W^{(kn)} F_1^{(k)} + \sum_{n=1}^{N_a} \frac{\partial \theta^{(n)}}{\partial x_i} \sum_{k=1}^{N_a} W^{(kn)} F_{2i}^{(k)}$$
$$+ \sum_{n=1}^{N_a} b^{(n)} \sum_{k=1}^{N_a} W^{(kn)} \Psi^{(k)},$$ (7)

$$\frac{\partial \theta(r)}{\partial x_i}\bigg|_{r=\xi} = \sum_{n=1}^{N_a} \theta^{(n)} \sum_{k=1}^{N_a} W^{(kn)} \frac{\partial F_1^{(k)}}{\partial x_i} + \sum_{n=1}^{N_a} \frac{\partial \theta^{(n)}}{\partial x_i} \sum_{k=1}^{N_a} W^{(kn)} \frac{\partial F_{2i}^{(k)}}{\partial x_i}$$
$$+ \sum_{n=1}^{N_a} b^{(n)} \sum_{k=1}^{N_a} W^{(kn)} \frac{\partial \Psi^{(k)}}{\partial x_i},$$ (8)

where N_a is the number of points used in the RBF approximations, $\theta^{(n)}$, $\partial\theta^{(n)}/\partial x_i$ and b_n are the values of $\theta(r)$, $\partial\theta(r)/\partial x_i$ and b at the nth approximation node and

$$F_1^{(k)} = \int_{\Gamma_s} f(r;r^{(k)}) \frac{\partial \Phi(r;\xi)}{\partial n} d\Gamma,$$

$$F_{2i}^{(k)} = \int_{\Gamma_s} f(r;r^{(k)}) \cdot n_i(r) \cdot \Phi(r;\xi) d\Gamma,$$ (9)

$$\Psi^{(k)} = \chi(r;r^{(k)})\big|_{r=\xi} - \int_{\Gamma_s} \chi(r;r^{(k)}) \frac{\partial \Phi(r;\xi)}{\partial n} - \Phi(r;\xi) \frac{\partial \chi(r;r^{(k)})}{\partial n} d\Gamma,$$

where $\chi(r;r^{(k)})$ is a particular solution associated with the chosen RBF. The coefficients $W^{(kn)}$ in (7) and (8) are explicitly given by

$$\sum_{n=1}^{N} W_{kn} f(r_n, r_m) = \begin{cases} 0, \text{ if } k \neq m, \\ 1, \text{ if } k = m, \end{cases} \quad \text{for } k, m = 1, 2, \ldots, N_a - 1, N_a.$$ (10)

Equations (7) and (8) form the basis behind the implementation of the RBIE.
For more details on the implementation of the RBIE, one may refer to Ooi and Popov [3] and Ooi et al. [4].

3   Numerical examples

The numerical results presented in this section were obtained by using the same set of nodes for the RBF approximations of the field variables and the DRM, see Figure 1b. In this case, $N_a = 25$ and 40 neighbouring nodes were used in the 2D and 3D problems, respectively. For the nodes that are at the global boundary, the unknown field variables that are exterior to the solution domain are extrapolated using the neighbouring nodes, see Figures 1c and 1d. All boundary integrations are numerically evaluated using the Gaussian quadrature after transforming the integration domain into the polar coordinate system. The functions $\Re^4 \log(\Re)$ and $\Re^3$ were used in the RBF approximations in the 2D and 3D examples, respectively [3, 4], where $\Re$ is the Euclidean distance between the field point and the interpolation point.

   To obtain a numerical solution, an iterative procedure that solves sequentially for each component of the velocity and vorticity vectors was developed. The iterative scheme is summarized as follows:

1.   Start with an initial guess (iteration level, $h = 1$) of the distribution of vorticity derivatives $\partial \omega_i^{(h-1)} / \partial x_j$.
2.   Solve the velocity Poisson equations for the distribution of the velocity vector $u_i^{(h)}$ and its spatial derivatives, $\partial u_i^{(h)}/\partial x_j$ using $\partial \omega_i^{(h-1)} / \partial x_j$.
3.   Calculate the boundary vorticity using the values of velocity gradients obtained from Step 2 by evaluating expression (2b).
4.   Using the values of $u_i^{(h)}$ and the boundary vorticity calculated in Step 3 as boundary conditions, solve the vorticity transport equation for the vorticity distribution $\omega_i^{(h)}$ and its spatial derivatives, $\partial \omega_i^{(h)}/\partial x_j$.
5.   Relax the vorticity and its spatial derivatives by using

$$\omega_i^{(h)} = \lambda \omega_i^{(h)} + (1-\lambda)\omega_i^{(h-1)},$$
$$\frac{\partial \omega_i^{(h)}}{\partial x_j} = \lambda \frac{\partial \omega_i^{(h)}}{\partial x_j} + (1-\lambda)\frac{\partial \omega_i^{(h-1)}}{\partial x_j}, \tag{11}$$

where λ is known as the relaxation parameter, which is a positive real number in the range of $0 \le \lambda < 1$.

6.   Check for convergence by calculating

$$\delta = \frac{\sum_{k=1}^{N_t}\left(\omega_{i,k}^{(h)} - \omega_{i,k}^{(h-1)}\right)^2}{\sum_{k=1}^{N_t}\left(\omega_{i,k}^{(h)}\right)^2}. \tag{12}$$

   If the value of δ is smaller than the pre-defined positive real number ε, then stop the iteration. Otherwise, repeat steps 1 to 6 for $h + 1$ by replacing the initial guess with the newly calculated values of vorticity. In the present study, ε is selected to be 10^{-5}.

3.1 Lid driven flow in a unit square cavity

The first example considered was a lid driven flow in a unit square cavity. The vertical and the horizontal bottom walls have a stationary no-slip condition such that $u_1 = u_2 = 0$, see Figure 2a. The top horizontal wall moves at a unit velocity in the positive x_1-direction, such that $u_1 = 1$ and $u_2 = 0$. Simulations were carried out using 441 uniformly distributed nodes.
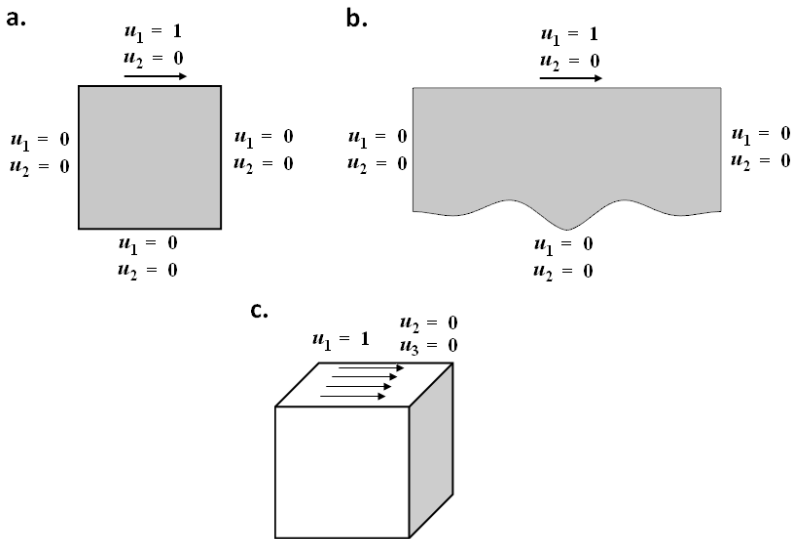

Figure 2: Geometrical sketch of the lid driven flows in a (a) unit square cavity; (b) rectangular cavity with wavy bottom and (c) unit cubic cavity.

Figures 3a and 3b compare the velocity in the x_1- and x_2-directions, respectively obtained using the RBIE and the FEM (with 6282 triangular elements). Very good agreement between the solutions of the RBIE and the FEM was observed. Figures 3c and 3d plot the profiles of the velocity vector and the vorticity distribution respectively, which agree with the results obtained by other researchers using other numerical methods [5, 6].

3.2 Lid driven flow in a rectangular cavity with wavy bottom

The lid driven flow in a rectangular cavity with a wavy bottom is considered, see Figure 2b. The rectangular cavity has width and height of 5 and 2, respectively, while the wavy bottom surface is described by the function $x_2 = -0.3\sin(\pi x_1)$ $[1 - (|x_1 - 2.5|)/2.5]$. The flow is driven by the top wall, which moves in the x_1-direction at unit velocity magnitude. All other boundaries have stationary no-slip condition. Simulation was carried out using 1139 uniformly distributed nodes.
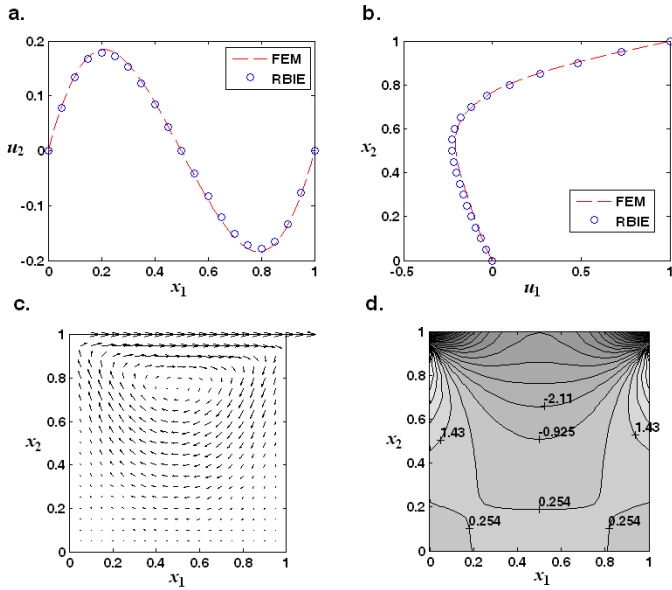
Figure 3:   Plots of (a) u_2 and (b) u_1 along the geometrical centre of the cavity and profiles of the (c) velocity vector and (d) vorticity distribution.
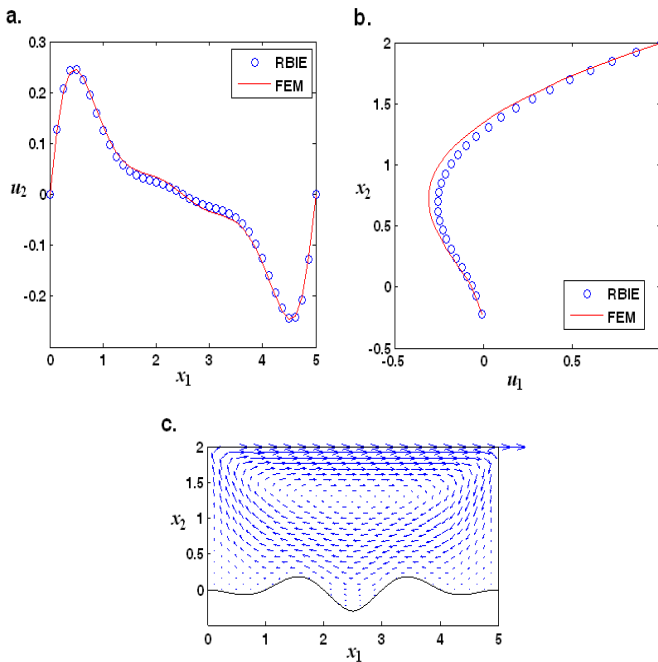

Figure 4:   Plots of: (a) u_2 at $x_2 = 1.08$; (b) u_1 at $x_1 = 2.5$, and (c) the velocity profile inside the rectangular cavity.

Figure 4a compares the values of u_1 and u_2 along $x_2 = 1.08$ and $x_1 = 2.5$ axes, respectively between the RBIE and the FEM (with 11069 triangular elements). There is a slight discrepancy between the solution obtained using the RBIE and the FEM for u_1 at points where the direction of the velocity changes. Very good agreement was found for u_2. The velocity vector inside the rectangular cavity is shown in Figure 4b, which agrees with those obtained by other researchers [6].

3.3 Lid driven cavity in a unit cubic cavity

A sketch of the unit cubic cavity is shown in Figure 2c. The top wall moves at a unit velocity in the x_1-direction. All the other walls have a no-slip stationary condition such that $u_1 = u_2 = u_3 = 0$. Simulations were carried out using 4913 nodes. Figures 5a and 5b compares the values of u_2 and u_1 obtained using the RBIE with the FEM (with 396832 tetrahedral elements) along the geometric centre of the cubic cavity, where one may observe good agreement between the numerical solutions of the RBIE and the FEM. Figure 5c plots the profile of the velocity vector inside the cubic cavity at $x_3 = 0.25$, 0.5 and 0.75. The 2D profile at $x_3 = 0.5$ is shown in Figure 5d. The results obtained compare well with those found in the literature [5].
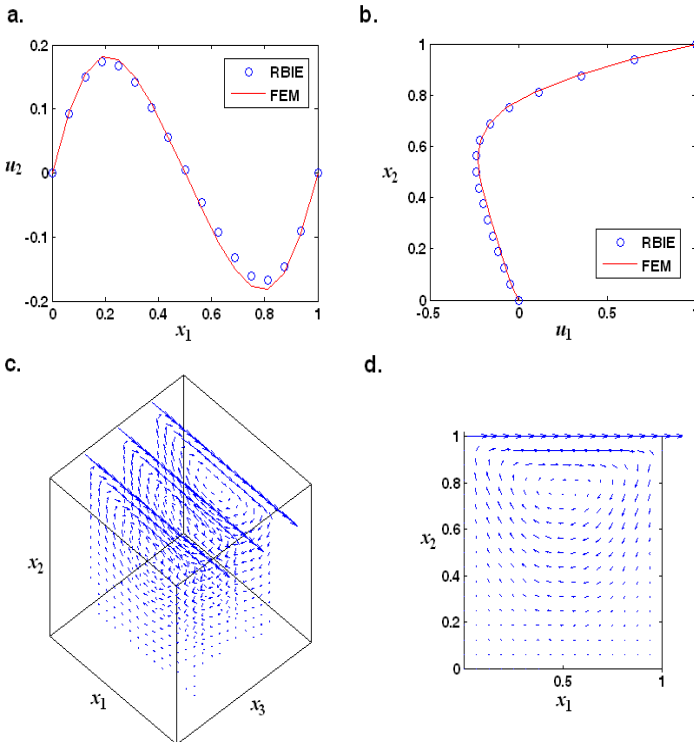

Figure 5:   Plots of (a) u_2 and (b) u_1 along the geometrical centre of the cavity; (c) profiles of the 3D velocity vector at $x_3 = 0.25$, 0.5 and 0.75; (d) profile of the 2D velocity vector at $x_3 = 0.5$.

4   Conclusions

The RBIE has been successfully implemented to solve 2D and 3D Stokes flow problems in the velocity-vorticity formulation. The RBIE is an appealing choice for handling such problems since the spatial derivatives of the velocity vector are obtained directly from the solution of the system of equations. In this way, the finite difference approximation that is commonly used in other numerical methods such as the finite difference method and the FEM can be avoided. In the numerical examples examined, the RBIE was found to be able to produce results that agree with the FEM when using significantly less number of degrees of freedom.

References

[1] Popov V. and Bui T.T., A meshless solution to two-dimensional convection-diffusion problems, *Engineering Analysis with Boundary Elements*, 2010; 34: 680–689.
[2] Partridge P.W., Brebbia C.A. and Wrobel L.C., *The Dual Reciprocity Boundary Element Method*, Computational Mechanics Publication, Southampton, 1992.
[3] Ooi E.H. and Popov V., An efficient implementation of the radial basis integral equation method, *Engineering Analysis with Boundary Elements*, 2012; 36: 716-726.
[4] Ooi E.H., Popov V. and Dogan H., Three-dimensional solution for acoustic and transport problems using the radial basis integral equation method, *Applied Mathematics and Computation*, 2012; accepted for publication.
[5] Young D.L., Jane S.C., Lin C.Y., Chiu C.L. and Chen K.C., Solutions of 2D and 3D Stokes laws using multiquadrics method, *Engineering Analysis with Boundary Elements*, 2004; 28: 1233-1243.
[6] Li X. and Zhu J., A meshless Galerkin method for Stokes problems using boundary integral equations, *Computer Methods in Applied Mechanics and Engineering*, 2009; 198: 2874-2885.